DOI: 10.1016/S1872-5805(21)60098-5

Two-dimensional layer materials for highly efficient molecular sensing based on surface-enhanced Raman scattering

YU Ling-xiao[1], LU Rui-tao[1,2,*]

(1. *State Key Laboratory of New Ceramics and Fine Processing*, *School of Materials Science and Engineering*, *Tsinghua University*, *Beijing* 100084, *China*;
2. *Key Laboratory of Advanced Materials (MOE)*, *School of Materials Science and Engineering*, *Tsinghua University*, *Beijing* 100084, *China*)

Abstract: Surface-enhanced Raman scattering (SERS) has been regarded as an attractive technique for efficient molecular sensing because of its nondestructive detection, fast response and high sensitivity. However, the majority of studies on SERS are still based on noble metals (e.g. Au, Ag), which suffer from the drawbacks of high-cost, low uniformity and poor stability, thus limiting their widespread use. Graphene shows an efficient SERS performance because of its two-dimensional (2D) atomically flat surface, large specific surface area, high stability and unique electronic/optical properties, which open up new avenues for SERS research. In recent years, other 2D inorganic layer materials, such as transition metal dichalcogenides (TMDCs), hexagonal boron nitride (h-BN), black phosphorus (BP), and MXenes, have also attracted increasing research attention. We summarize the SERS mechanisms and state-of-the-art progress on substrates based on 2D materials, including graphene and other 2D inorganic layer materials. The challenges and prospects for future research on high-performance SERS substrates are considered.

Key words: Graphene; SERS; Enhancement mechanism; Molecular sensing

1 Introduction

Since C.V. Raman reported the scattering phenomenon in 1928, Raman scattering has been regarded as a promising analytical technology, however the poor intensity of Raman signal caused by the lack of inelastic scattered photons restricts its wide applications[1]. In 1974, the discovery of surface-enhanced Raman scattering (SERS) on rough silver surface by M. Fleishman *et al.* contributed to enhancing scattering intensity several orders of magnitude[2], remarkably broadening its utilizations on molecular sensing, such as environmental monitoring[3], food safety[4], disease diagnosis[5], biosensing[6], and molecular fingerprint recognition[7]. Besides, because of the shorter vibrational relaxation time than that of electron, there are higher emitted rate of Raman photons by a molecule than fluorescence photons, which makes it promising for single molecular detection with high sensitivity for SERS[8]. In virtue of noncontact, nondestructive detection, rapid response and high sensitivity, SERS has attracted numerous efforts of researchers on developing novel SERS substrates with higher sensitivity, better uniformity and reproducibility[9–12]. To date, noble metals, such as Au and Ag, are main materials served as SERS platforms with high performance, which however suffer from high-cost, low surface uniformity, poor stability, strong spectral background and even arising side catalytic reactions for too strong interaction with probe molecules sometimes, thus hindering their further scale-up applications[13]. In this context, it is crucial to develop noble-metal-free SERS-active substrates for future widespread applications.

Recently, graphene and other 2D inorganic layered materials, such as transition metal dichalcogenides (TMDCs), hexagonal boron nitride (h-BN), black phosphorus (BP), MXenes, *et al.*, have been investigated as possible candidates for SERS substrates for molecular sensing to overcome the drawbacks of noble metals with large specific surface areas, unique electronic and optical properties, atomic uniformity, biological compatibility and high stability (Fig.1)[14]. However, there are still few studies on 2D inorganic layered nanomaterials served as alternative SERS substrates compared with noble metals and less experi-

Received date: 2021-08-09; **Revised date:** 2021-10-28

Corresponding author: LU Rui-tao, Associated Professor. E-mail: lvruitao@tsinghua.edu.cn
Author introduction: YU Ling-xiao, Ph.D candidate. E-mail: ylx20@mails.tsinghua.edu.cn

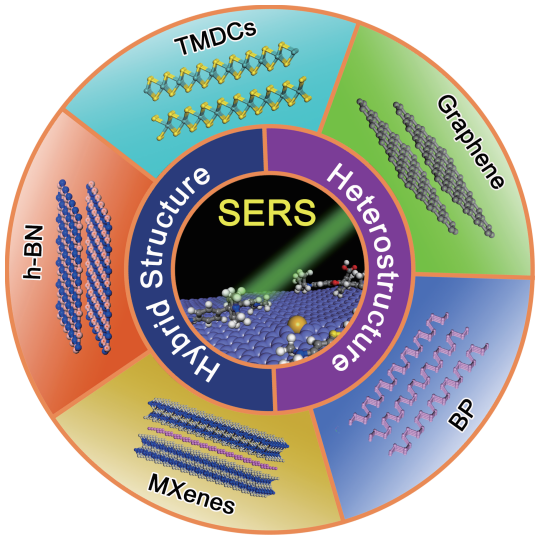

Fig. 1 Various inorganic 2D layered materials for surface-enhanced Raman scattering (SERS). Here h-BN denotes hexagonal boron nitride. TMDCs and BP denote transition metal dichalcogenides and black phosphorus, respectively.

ence has been accumulated to guide further development. In this article, we will focus on the recent development and enhancement mechanism of 2D inorganic layered materials for molecular sensing. Then we will emphasize the factors on SERS performance in details, which will be insightful for tuning the properties of substrate materials. Finally, we propose the challenges ahead based on current advances of 2D inorganic layered materials and perspectives for future development.

2 Enhancement mechanisms for SERS

Raman signal arises from the inelastic scattered photons (i.e. the Stokes scattering and Anti-Stokes scattering) when the incident photons irradiates on the samples. As shown in Fig. 2a and b, it can be roughly divided into two steps: a few incident photons gain (or lose) energy when they interact with samples and then scatter with more (or less) energy, in which the change of the energy is called as Raman shift[10, 15]. As for molecular sensing, the incident light will induce a dipole moment (μ) into the probe molecule, of which the square is proportional to the Raman intensity (I), expressed as[11]:

$$I \propto \mu^2$$

Thus, the Raman signal can be amplified through enhancing the dipole moments of the molecules, such as increasing the incident electromagnetic field surrounding the molecules and promoting the polarization of the molecules. Up to now, there are two mechanisms of enhancement for Raman scattering accepted generally, the electromagnetic mechanism (EM)

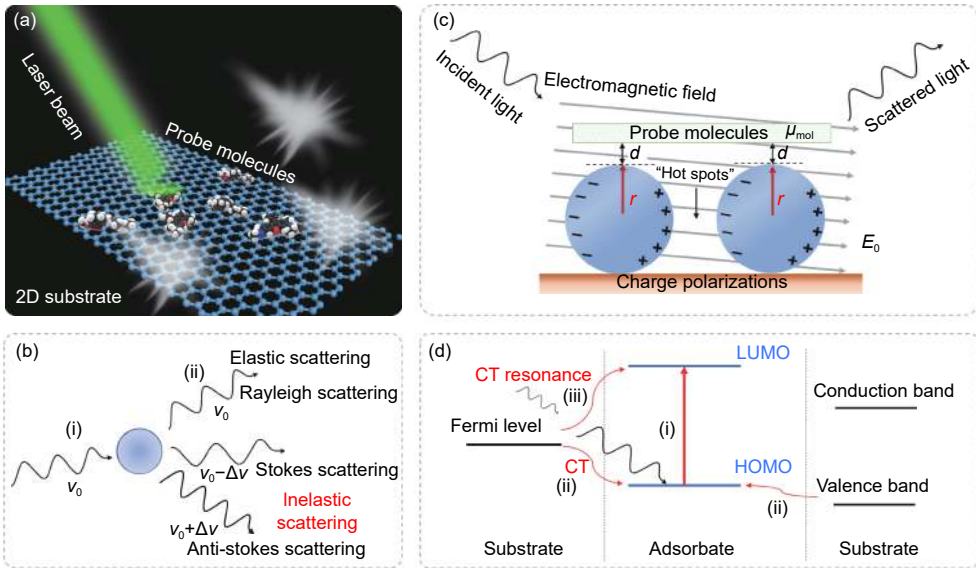

Fig. 2 Schematic illustrations of (a) SERS, (b) mechanism of Raman scattering (v_0 and Δv represent the frequency of incident light and the change of frequencies after scattering, respectively), (c) electromagnetic mechanism (EM) and (d) chemical mechanism (CM) for SERS (Here E_0 is the incident electromagnetic field, μ_{mol} is the induced dipole moment of probe molecule, r is the radius of the metal spheres and d is the distance between the probe molecule and the surface of metal sphere, CT represents the charge transfer, HOMO and LUMO denote the highest occupied molecular orbital and the lowest unoccupied molecular orbital, respectively).

and the chemical mechanism (CM)[14].

2.1 Electromagnetic mechanism (EM)

Electromagnetic mechanism has been studied more thoroughly than others and it has been widely used to explain the enhancement of Raman signal on the metallic surface by an amplified incident electromagnetic field. As shown in Fig. 2c, there will be an incident electromagnetic field emerged by the incident light, generating induced dipole moments ($\boldsymbol{\mu}^0_{\mathrm{mol}}$) for the probe molecules, which is determined by the polarizability of the molecule (α_{mol}) and the incident electromagnetic field ($\boldsymbol{E}_0(\omega)$) as below[16] :

$$\boldsymbol{\mu}^0_{\mathrm{mol}} = \alpha_{\mathrm{mol}} \cdot \boldsymbol{E}_0(\omega)$$

It can be simply described that metal nanospheres are exposed in the applied electromagnetic field and the oscillating electromagnetic field will excite the electrons in the metal spheres leading to polarizations of charges and inducing dipole moments[15]. When the angular frequency of the induced dipole moments is equal to that of the incident light, there will be a significant enhancement for local electromagnetic field on the surface caused by local resonance effect, called localized surface plasmon resonance (LSPR)[17]. Therefore, while the molecules approach the surface of the metal spheres, they can be polarized by a stronger local electromagnetic field (E_{loc}), which can be expressed as[15]:

$$E_{\mathrm{loc}} = E_0 \cos\theta + \left(\frac{r^3}{d^3}\right) E_0 \cos\theta$$

where θ is the angle relative to the direction of the electric field, r is the radius of the metal spheres and d is the distance between the probe molecule and the surface of metal sphere, so that an enhancement of Raman intensity can be obtained due to the larger dipole moments $\mu^{\mathrm{loc}}_{\mathrm{mol}}$ given as:

$$\mu^{\mathrm{loc}}_{\mathrm{mol}} = \alpha_{\mathrm{mol}} \cdot E_{\mathrm{loc}}$$

Furthermore, the Raman signal of the probe molecule can be considered as[16],

$$I_{\mathrm{SERS}} \propto |E_{\mathrm{inc}}|^2 \cdot |E_{\mathrm{sca}}|^2 \approx |E_{\mathrm{inc}}|^4$$

where I_{SERS} represents the intensity of the Raman signal, E_{inc} and E_{sca} are regarded as the fields from the incident light and the scattering light respectively. Therefore, the electromagnetic enhancement factor (EEF) is approximately proportional to the fourth power of the ratio of the local electromagnetic field to the incident electromagnetic field, which can be expressed as:

$$EEF \propto |E_{\mathrm{loc}}/E_0|^4$$

Generally, the orders of magnitude of the enhancement factor can be up to 8 or even larger[18, 19]. Indispensably, it is worthy to note that the most intense scattering arises not from the metal particle itself but in the gaps between the surrounding particles to bring large enhancement in most cases, which are usually called as “hot spots”[15].

2.2 Chemical mechanism (CM)

Chemical mechanism (CM) is more ambiguous compared to electromagnetic mechanism, there is still no specific and concrete consensus to comprehensively explain the process of CM. Encouragingly, with the further studies on plasmon-free SERS materials and fast advances of computer simulation technology, chemical mechanism has been elucidated gradually[9, 10, 19]. Chemical mechanism for SERS is dependent on the electronic structure of the interface between the probe molecules and the substrates, thus the probe molecule layer closest by the substrate is the key factor for CM, which is regarded as “first layer effect” generally[11]. There are three forms of chemical mechanism: (1) the probe molecules interact with the substrate by chemical bonds. (2) the probe molecules form coordination compounds with the SERS substrate. (3) charge transfer occurs between the probe molecules and the SERS substrate. Among them, it is notable that the charge transfer (CT) mechanism tends to occur between the adsorbed molecules and 2D inorganic layered material SERS substrates. According to frontier molecular orbital theory, the electrons in molecules can be divided into different molecular orbital energy levels for different energies[20], among which the highest occupied molecular orbital (HOMO) and the lowest unoccupied molecular orbital (LUMO) are the keys to the interaction with other matters. Fig. 2d illustrates the charge transfer mechanism for SERS, the electrons in the HOMO levels of the probe molecules can be excited to the LUMO levels by the incident light (Fig. 2d(i)), then the electrons may mi-

grate from the valence band (VB) or Fermi level of substrates to the HOMO levels of the probe molecules and recombine with remaining holes (Fig. 2d(ii))[21], in which according to the Fermi's golden rule, the electron transition probability rate w_{lk} can be given as[22]:

$$w_{lk} = \frac{2\pi}{\hbar} g(E_k)|H'_{kl}|^2$$

where $g(E_k)$ is the density of the states (DOS) and H'_{kl} represents the matrix element for a transition from LUMO to HOMO. Therefore, the Raman enhancement is determined by the DOS and the matrix element of different substrate materials, which can be tailored by the position of the energy levels and the interfacial interaction[21]. Besides, the Raman signal can be also dramatically enhanced by charge transfer resonance when the energy gap between the energy level of the substrates (taking the Fermi level as an example in Fig. 2d(iii)) and LUMO or HOMO levels of the probe molecule is close to the energy of the laser[23]. In addition, the interfacial dipole-dipole interaction can also improve the polarization of the probe molecules to increase the final Raman signal. Thus, the total dipole moments of the molecule in the chemical mechanism can be simply expressed as[24]:

$$\boldsymbol{\mu}_{mol}^{loc} = \boldsymbol{\mu}_0 + \boldsymbol{\mu}_{loc}$$

Here $\boldsymbol{\mu}_0$ and $\boldsymbol{\mu}_{loc}$ are the dipole moments induced by incident light and substrates, respectively. In general, the enhancement factor of chemical mechanism is about 10^0–10^2, which is much weaker than that of electromagnetic mechanism. But inspiringly, there are also many works on 2D layered material SERS substrates verified to have ultra-high sensitivities and low limit of detection recently by tuning the electronic structures and properties with various methodologies.

3 2D inorganic layered materials for sensing

3.1 Graphene

Graphene, the star of 2D inorganic layered materials, is a monolayer sp^2-hybridized carbon atoms arranged into honeycomb-like skeletons, which has attracted vast attentions of researchers over the past decades[25]. Since it was discovered in 2004[26], graphene has been employed in various fields due to its large specific surface area, atomic uniformity, excellent mechanical capacities, high stability and good biocompatibility, as well as unique and tunable electronic and optical properties[14, 27–28]. Recently, graphene has also been demonstrated as an active SERS substrate with an efficient fluorescence quenching ability and enhancement for Raman signal of some dye molecules, such as rhodamine B (RhB), crystal violet (CV), methylene blue (MB), phthalocyanine (Pc) and so on, by chemical mechanism, which is also termed as graphene-enhanced Raman scattering (GERS) effect[29, 30]. So far, there are two models of charge transfer mechanisms for chemical enhancement, the ground-state and the excited-state mechanisms. In order to investigate the type of charge transfer mechanism in GERS, Ling *et al.*[31] tested the Raman spectra of CuPc under different laser wavelengths and they found that there was no charge-transfer resonance peak at about 1.9 eV, which is not consistent with the excited-state model, identifying a ground-state charge transfer mechanism in GERS. For further understanding of GERS, the factors responsible for enhancement factor of GERS can be considered from three aspects: graphene, the probe molecule and the incident laser.

Graphene is a zero-band-gap semiconductor and its Fermi level tends to locate between the LUMO and HOMO levels of dye molecules generally, which can be tuned *via* various strategies, such as electrical field effect (EFE), chemical doping, defect engineering and so on[23, 32–35]. For example, Xu *et al.*[23] demonstrated an electrical field modulation method to tune the Fermi level of graphene by electrical field effect and they found that the Fermi level could be down-shifted by a negative gate voltage due to the EFE-induced hole doping, whereas up-shifted due to the electron doping, as shown in Fig. 3a. It was reported that the downshifted Fermi level made the energy gap between the LUMO level of the CoPc molecule and the Fermi level of graphene close to the laser energy, thus leading to a charge transfer resonance process, which efficiently enhanced the Raman intensity. Re-

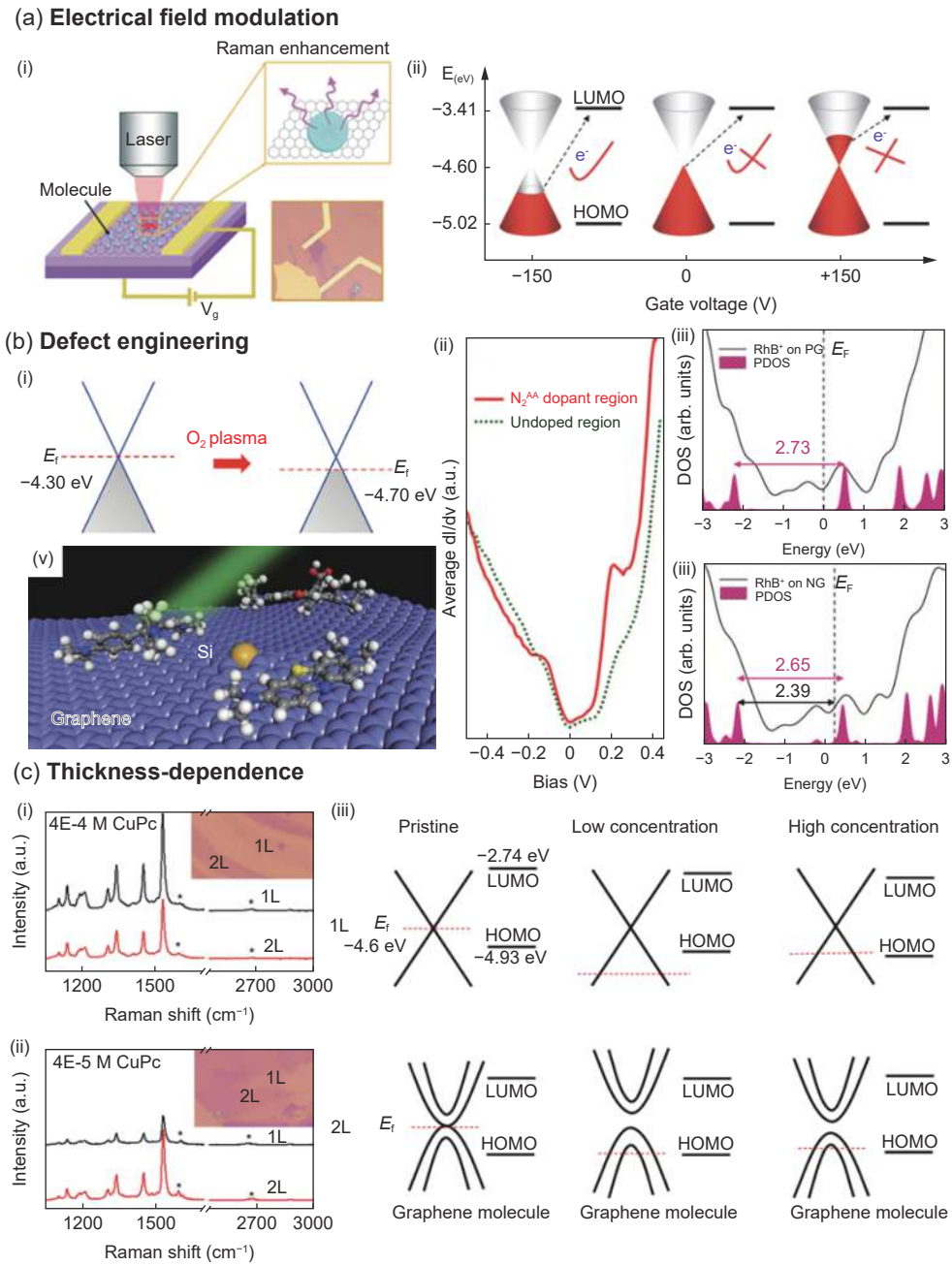

Fig. 3　(a) Electrical field modulation on Fermi level for graphene-enhanced Raman scattering (GERS). (i) Schematic diagram of the device on tuning the graphene Fermi level by electrical field effect. (ii) The energy level alignment between the molecular energy level and modulated graphene Fermi level for charge transfer resonance[23] (reprinted with permission from American Chemical Society). (b) Defect engineering for GERS. (i) Schematic illustrations of the Fermi level modulation by O_2 plasma treatment[33] (reprinted with permission from Elsevier). (ii) the dI/dV curves (averaged over 9 points spectra taken in 1×1 nm^2 area) measured on N_2^{AA} dopants and undoped graphene[25] (reprinted with permission from Spring Nature). The density of states (DOS) for Rhodamine B (RhB) on (iii) the pristine graphene (PG) and (iv) N-doped graphene (NG), E_F represents the Fermi level[14] (reprinted with permission from AAAS), (v) Schematic of SERS on Si-doped graphene[32] (reprinted with permission from John Wiley and Sons). (c) Thickness-dependence of GERS. (i-ii) Raman spectra of copper phthalocyanine (CuPc) molecule and (iii) schematic illustration of the energy band structure of mono- and bilayer graphene under low and high concentration molecular solution[36] (reprinted with permission from American Chemical Society).

cently, plasma-based technique has been proved as an elaborate route to decorate graphene. There exist strong local dipoles with oxygenated species on treated surface and down-shifted Fermi level of graphene by an O_2 plasma treatment (Fig. 3b(i)). The local dipoles may promote the polarization of the probe molecule for strong interaction with substrate. And the down-shifted Fermi level can cause a charge

transfer resonance with laser energy, thus resulting in a large chemical enhancement. Indeed, the limit of detection (LOD) of RhB can be reduced to 10^{-7} mol L^{-1} after the treatment with O_2 plasma for graphene, greatly amplified compared with that of pristine graphene[33]. More importantly, substitutional doping is also a very promising way to tailor the electrical and chemical properties of graphene. Our group investigated a remarkable enhanced Raman scattering with an effective fluorescence quenching effect on N-doped graphene (NG) substrate, mainly due to the higher density of states (DOS) and more suitable tailored energy gaps in NG than the pristine graphene (PG) (Fig. 3b(ii-iv)), thus facilitating charge transfer resonance in the system and resulting in a low detection level of 5×10^{-11} mol L^{-1} for RhB[14, 25]. Furthermore, we found that Si-doped graphene reached an even better SERS performance than NG and PG for detecting different dyes, including CV, RhB and MB. Si-dopants can not only change the DOS and Fermi level of graphene like NG but also induce local curvature around the substitutional sites for much larger volume of silicon atom than carbon (Fig. 3b(v)), thus promoting the interaction between the probe molecules and graphene substrates[32].

In fact, it is not easy to obtain "true" graphene with just one layer, it is common to get bilayer and multilayer graphene sheets in most cases. Ling *et al.*[36] found that graphene was a thickness-dependent SERS substrate and determined by concentration of molecular solution *via* solution soaking method. They demonstrated that the enhancement factor generally decreased with the increase of the layer number in most cases. However, it is interesting in Fig. 3c (i) and (ii) that bilayer graphene showed a stronger Raman intensity than monolayer graphene under low concentration solutions (4×10^{-5} mol L^{-1}) for CuPc detection, whereas there was little difference between them in high concentration (4×10^{-4} mol L^{-1}). It can be explained that *p*-doping is induced in the graphene with a downshifted Fermi level when the CuPc molecule attached the graphene and there was similar change in Fermi level positions of mono- and bilayer graphene at high concentration with similar energy gaps for charge transfer. They also found that monolayer graphene is more sensitive to dope than bilayer graphene, thus resulting in a larger decline of Fermi level at low concentration. So that, the Fermi level of the monolayer graphene will be much lower than the HOMO of the CuPc molecule (Fig. 3c (iii)), thus the charge transfer needs extra energy to emerge, while there is less reduction of the Fermi level in bilayer graphene and the Fermi level still keep higher than the HOMO level of the molecule, thus facilitating charge transfer without extra energy. Besides, the stacking configuration of bilayer graphene can also affect the enhancement effect for molecule sensing, it was indicated that rotated graphene could detect the MB under low concentrations about 10^{-6} mol L^{-1} whereas AB stacking seemed to be insensitive for MB molecule[37]. In general, high quality and clean surface are beneficial for graphene to gain superior sp^2 carbon domain, which greatly dominates the fluorescence quenching effect[38]. With quantum confinement and edge effect, high-quality graphene quantum dots prepared by plasma-enhanced chemical vapor deposition (P-GQD) demonstrated a high enhancement for SERS of sensitivity down to 1×10^{-9} mol L^{-1} rhodamine with good fluorescence quenching and its enhancement factors were up to 437 (1 648 cm^{-1} Rhodamine 6G (R6G)), about 7 times higher than that on CVD graphene (Fig. 4a). It is clarified by DFT calculation that the band gap increases with the decreasing of the diameter of the GQDs and there is a more sufficient charge transfer between the molecule and P-GQD than on perfect graphene with higher DOS, especially when the size is about 6.2 nm, leading to a larger polarizability and the higher Raman scattering cross-section for great enhancement effect[39].

In essence, the enhancement of Raman intensity mainly relies on the relation between the Fermi level of the graphene and the HOMO or LUMO levels of the probe molecules, therefore it is also important to take the properties of the probe molecules into consideration for GERS performance. There are two key factors of molecules carried out to have influence on the final GERS effect: (1) the distinct alignments of HOMO and LUMO energy levels and (2) various mo-

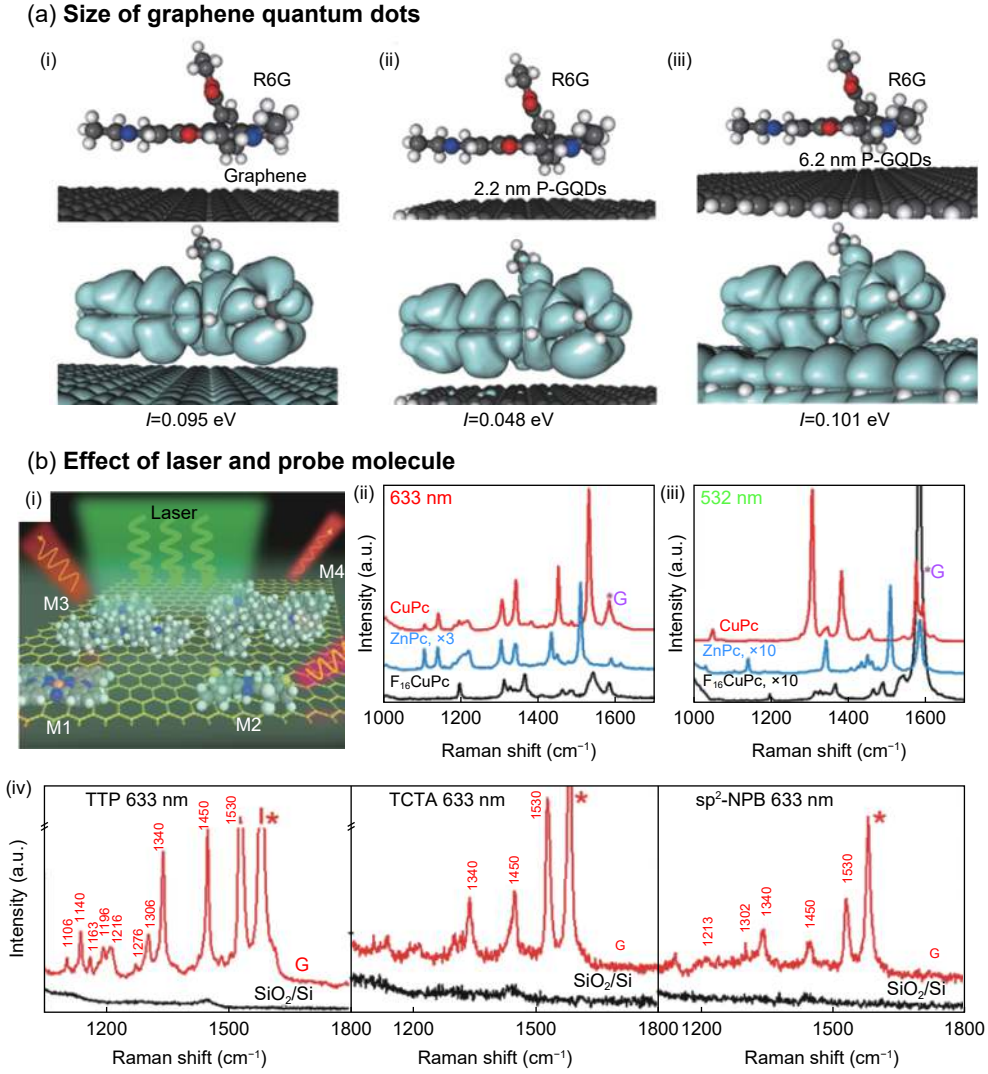

Fig. 4　(a) The influence of size of graphene quantum dots on GERS. The calculated charge transfer integrals (I) of rhodamine 6G (R6G) with (i) pristine graphene and high-quality graphene quantum dots prepared by plasma-enhanced chemical vapor deposition (P-GQDs) of (ii) 2.2 nm and (iii) 6.2 nm sizes[39] (reprinted with permission from Spring Nature). (b) Impact of molecule and laser energy. (i) Schematic illustration of the influence of molecule and laser on GERS (here M1–M4 represent four different molecules). Raman spectra of CuPc, zinc phthalocyanine (ZnPc), and copper(II)1,2,3,4,8,9,10,11,15,16,17,18,22,23,24,25-hexadecafluoro-29H,31H-phthalocyanine (F_{16}CuPc) under (ii) 532 nm and (iii) 633 nm laser. (iv) Raman spectra of tetrathienophenazine (TTP), tris(4-carbazoyl-9-ylphenyl) amine (TCTA), and 2,2′,7,7′-tetra(N-phenyl-1-naphthyl-amine)-9,9′-spirobifluorene (sp^2-NPB) on graphene[40] (reprinted with permission from American Chemical Society).

lecular structures of various probe molecules. It can be explained by the time-dependent perturbation theory that the enhancement effect required the HOMO and LUMO levels to be suitable range with respect to the Fermi level of graphene, which determined the emergence of SERS. Besides, the similar symmetry of the molecules and graphene (D_{6h}) is more likely to yield a better GERS performance. We can inferred from Fig. 4b(iv) that tetrathienophenazine (TTP) (D_{2h}) exhibited about 3.4 times and 5.4 times higher GERS enhancement factor than that of tris(4-carbazoyl-9-ylphenyl) amine (TCTA) (C_3) and 2,2′,7,7′-tetra(N-phenyl-1-naphthyl-amine)-9,9′-spirobifluorene (sp^2-NPB) (S_4), respectively, with the similar HOMO/LUMO energy arrangements[40]. In addition, due to the large delocalized π electron cloud of graphene, when the π orbitals in molecule couple with graphene at a certain orientation, there may be larger interfacial dipoles and electron transition relying on the π-π interaction, thus definitely facilitating stronger GERS intensity[41].

Moreover, laser energy will also have a remark-

able influence on GERS. In our previous work, we found that different dye molecules had different resonant laser lines to achieve the best enhancement result, for instance, 514.5 nm laser line for CV and RhB and 647 nm laser line for MB[32]. And we believed that the strongest Raman signal could be achieved when the laser energy is close to the HOMO-LUMO gap of the molecule[14]. Similarly, Huang *et al.*[40] made comparisons between 633 nm and 532 nm laser energies on different probe molecules (Fig. 4b(i-iii)) and they demonstrated that strong GERS enhancement generated when the laser energy is close to the HOMO-LUMO gap or the energy gap between the Fermi level of graphene and the HOMO or LUMO levels of the probe molecules due to higher Raman scattering efficiencies according to the perturbation theory and Fermi's golden rule.

The successful exploration on graphene served as active-SERS substrates has opened up new avenues for molecular sensing on manifest 2D inorganic layered materials beyond graphene, including TMDCs, h-BN, BP, MXenes and so on, which will be discussed in the following sections.

3.2 Transition metal dichalcogenides

Transition metal dichalcogenides, with sandwich structures, have been also demonstrated as attractive platforms for SERS due to the large specific surface area, tunable electron structure and extraordinary optical properties. In general, the transition metal atoms (M) always arrange between the two layers of chalcogen atoms (*X*), usually denoted as MX_2, which could accelerate charge transfer process through M-X bonds and cause large interfacial polarization due to the difference in electronegativities of atoms[42–44]. Therefore, the enhancement of Raman signal can be attributed to the large interaction with probe molecules through not only charge transfer but also interfacial dipole-dipole interactions. For example, our group synthesized single crystal NbS_2 with atomically flat surface controllably by chemical vapor deposition (CVD) method and the as-grown NbS_2 demonstrated much higher sensitivity for probing trace than that of graphene[45].

Different TMDCs have been studied on SERS in the past years and most of them have been confirmed to be practicable substrates with impressive SERS performance. For example, Tao *et al.*[46] employed the 1T'-WTe_2 on R6G detection and the substrate exhibited a high sensitivity with the EF of 4.4×10^{10} and the LOD of 4×10^{-15} mol L^{-1}, better than most of graphene-based substrates ascribed to the higher DOS and more favorable charge transfer with the probe molecule, which can be seen in Fig. 5a and b. Additionally, they also tested the sensing performance of 1T'-WTe_2, the substrates exhibited ultra-high sensitivity as well with low LOD of 4×10^{-14} mol L^{-1} R6G and EF of 6.2×10^{9}. Likewise, 1T'-$MoTe_2$ films, prepared *via* CVD possessed superior capacities of molecular detection for biosensing with a LOD of 10^{-9} mol L^{-1} and an enhancement factor of about 10^4 on *β*-sitosterol. It is noteworthy that the $MoTe_2$ films also demonstrated an outstanding linear correlation between the intensity (at the peak of 1 668 cm^{-1}) and concentration logarithm with a coefficient of 0.998 8, showing a promising SERS substrate for quantitative biosensing[6].

Besides 1T'-phase, there are always three other main types: hexagonal phase (2H), trigonal phase (1T) and rhombohedral phase (3R)[47–49]. Different phases tend to have different electron structures, thus affecting SERS results. Yin *et al.*[21] investigated the difference between semiconducting 2H-MoX_2 and metallic 1T-MoX_2 (*X* = S, Se) and pointed out that the Raman enhancement effect could be increased *via* a phase transition from 2H- to 1T-phase (Fig. 5c). The energy levels can be represented as Fermi levels and valence bands (VB) and conduction bands (CB) in 1T- and 2H-phase, respectively, out of the different electronic properties. In virtue of the higher position of Fermi level than that of the top of VB (TVB), it is easier for electrons in 1T-phase to transfer to the HOMO level of the probe molecule (Fig. 5d). Besides, as for the case of the excited state, in which the electrons are probably excited from the HOMO level of the molecule to the CB/Fermi level of the substrate. As shown in Fig. 5e, smaller energy gap between Fermi level of 1T'-phase and HOMO level of the MB molecule contributes to more effective electron migra-

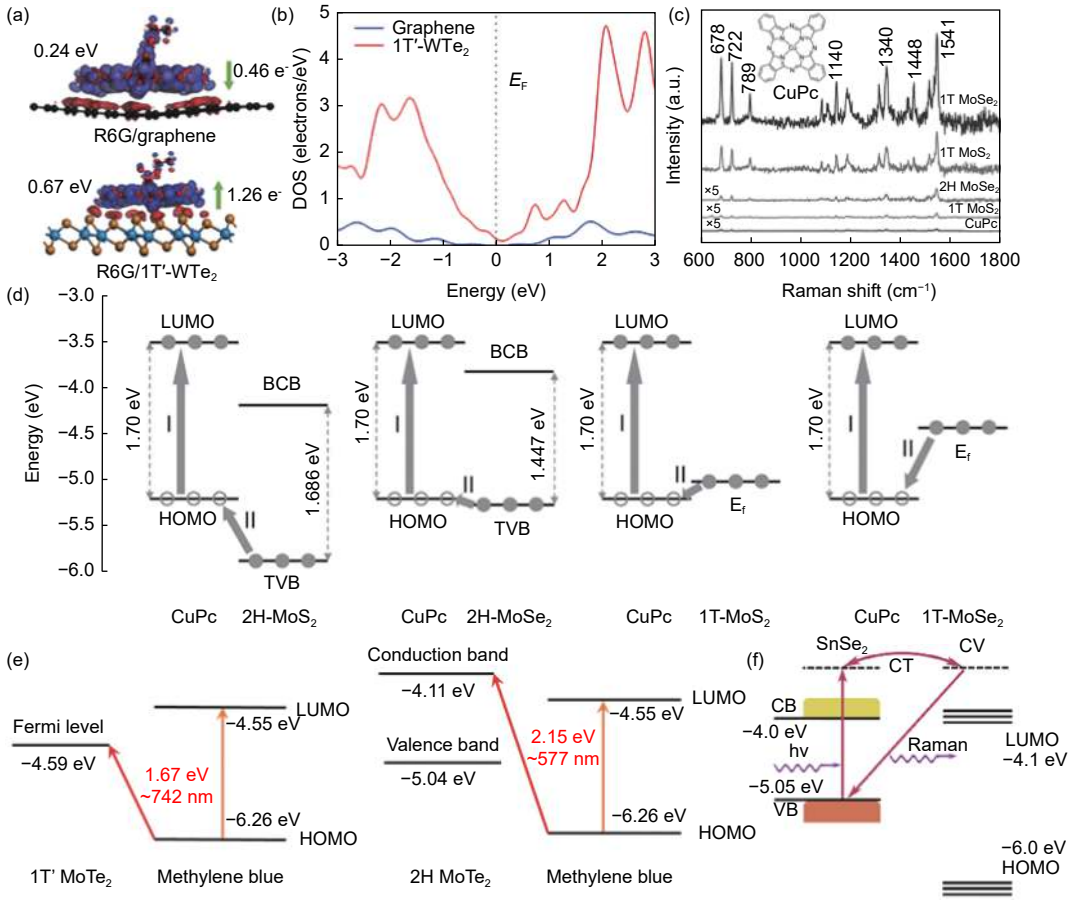

Fig. 5　(a) The electron density difference isosurfaces for R6G on graphene and 1T'-WTe_2. (b) DOS of 1T'-WTe_2 and graphene [46] (reprinted with permission from American Chemical Society). (c) SERS spectra and (d) schematic illustration of charge transfer mechanism of CuPc on different substrates[21] (reprinted with permission from John Wiley and Sons). (e) Schematic illustration of energy level and charge transfer resonance process for SERS of MB on 1T'- and 2H $MoTe_2$[50] (reprinted with permission from IOP). (f) Schematic illustration of energy level and charge transfer process for SERS of crystal violet (CV) on $SnSe_2$[52] (reprinted with permission from John Wiley and Sons).

tion with lower excited energy than that of 2H-phase[50]. Hence, metallic TMDCs have tendency to obtain higher Raman intensity because of its more suitable energy levels. However, some novel semiconducting TMDCs still perform excellent enhancement effect. $SnSe_2$, a semiconductor with a bulk bandgap of about 1.05 eV, was claimed to detect R6G with the ultralow concentration of 10^{-17} mol L^{-1} due to the matched energy level (−5.05 eV of VB and −4.0 eV of CB) with the HOMO/LUMO levels of the probe molecule to drive charge transfer, especially the unusual high VB level (Fig. 5f)[51, 52].

The bulk TMDCs generally have indirect band gap, which can be transformed into direct band gap when reduced to monolayer, thus most of TMDCs display thickness-dependent SERS performance like graphene[43]. For example, Meng *et al.*[53] prepared WS_2 ranging from monolayer to bulk-layer by CVD. They found that the single layer WS_2 offered the strongest Raman intensity of R6G and the Raman enhancement effect decreased with the increase of the layer numbers due to the indirect relaxation process. Moreover, the metallic 2D NbS_2 monolayer synthesized by Song *et al.*[54] demonstrated a detection limit down to 10^{-14} mol L^{-1}, much lower than that of 1T-MoS_2 and graphene, because the high DOS led to an increased intermolecular charge transfer probability. It was reported that the amount of the 2H phase, which was verified higher DOS than that of 3R phase, increased with the decrease of the layer number, hence NbS_2 with fewer layers exhibited larger Raman enhancement. Besides, ReS_2 always crystallizes in distorted octahedral (1T') with in-plane anisotropic optoelectronic properties, its Raman enhancement effect is

still sensitive to the thickness with the direct-indirect bandgap transformation and the single-layer ReS_2 showed a detection limit as low as 10^{-9} mol L^{-1}. Nevertheless, as shown in Fig. 6a, the fluorescence background signal will also increase with the decrease of the layer number, hindering its further applications[55]. Interestingly, it was reported by Wang *et al.*[56] that the underlying substrate for ReS_2 films might play roles on fluorescence quenching effect. They found that monolayer ReS_2 on mica expressed obvious fluorescence quenching compared to ReS_2 on SiO_2 and quartz (Fig. 6b and c). Electrons tend to transfer from the SiO_2 substrate to ReS_2, resulting in electron doping to restrict the electron transformation from LUMO level of the molecule to CB of ReS_2, which is fundamental to the fluorescence quenching, while no electron doping exists on mica for its inert surface. Furthermore, due to the high flexibility, the ReS_2 films on mica showed a good robustness after bending for 1 000 times, which is beneficial for their applications in flexible devices. Our group elucidated the influence of thickness on Raman enhancement for $NbSe_2$. Large-area $NbSe_2$ flakes ranging from multilayer to monolayer was synthesized controllably by ambient pressure CVD. Different from most of researches, the $NbSe_2$ with 6 layers was demonstrated a five orders of magnitude lower LOD of 5×10^{-16} mol L^{-1} than that of monolayer $NbSe_2$ (Fig. 6d and e). The DFT calculation indicates that the as-grown $NbSe_2$ flakes could contribute to strong interaction with R6G and the 6L-$NbSe_2$ possessed the highest DOS value at the Fermi level, giving rise to the most efficient charge transfer process for SERS by chemical mechanism (Fig. 6f)[57]. Indeed, it can be found that the electron structure, such as energy levels and DOS, is the main factors of the thickness-dependence phenomenon. Defect engineering is also a promising strategy to tailor electron structure of materials. Liu *et al.*[44] tuned the atomic ratio of WSe_2 monolayers by Au ion beam to obtain an optimized SERS substrate, which can be seen in Fig. 7a. And the atomic ratio (Se:W) can be tailored from 1.92 to 2.00 by different controlled dose/fluence (S_1=10^{12} ions cm^{-2}, S_2=10^{13} ions cm^{-2}, S_3=10^{14} ions cm^{-2}) of ion beam (Fig. 7b). They found that the EF was increased to more than 40 times on WSe_2 monolayer with the atomic ratio of 1.96 than the pristine WSe_2 (Fig. 7c). According to fs optical pump-probe spectroscopy (Fig. 7d), the quantity of the exciton increased by about 9 times, which is beneficial to the enhancement effect. And it was confirmed by DFT

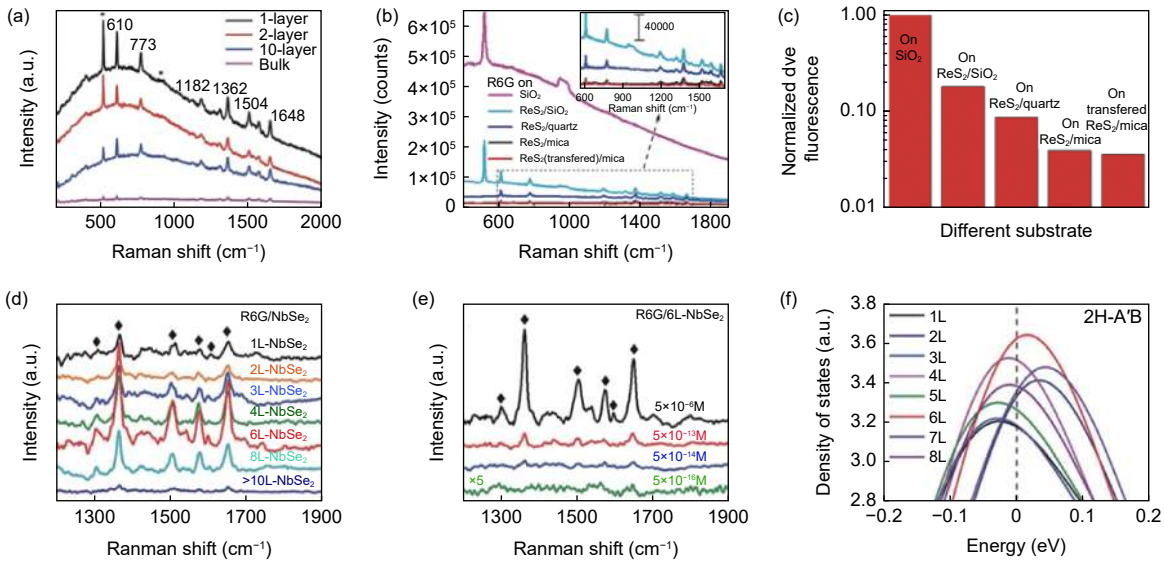

Fig. 6 (a) SERS spectra of 10^{-6} mol L^{-1} R6G on different layer number ReS_2 films[55] (reprinted with permission from John Wiley and Sons). (b-c) SERS spectra and normalized fluorescence of R6G on monolayer ReS_2 with different underlying substrates[56] (reprinted with permission from Elsevier). SERS spectra of R6G (d) with 5×10^{-6} mol L^{-1} on $NbSe_2$ with different layer numbers and (e) on 6L-$NbSe_2$ with different R6G concentrations. (f) DOS of the outermost layer of 2H-$NbSe_2$ with different layers in the A'B stacking mode[57] (reprinted with permission from Royal Society of Chemistry).

that the total density of states (TDOS) increased with the decrease of atomic ratio, as shown in Fig. 7e.

There are also other strategies to further improve the SERS performance for TMDCs. Chen *et al.*[58] fabricated vertically-aligned MoS_2 and WS_2 nanosheets on metal foils with mixed 1T and 2H phase by a hydrothermal reaction. The SERS measurements showed that the detection limits of both MoS_2 and WS_2 can attain 5×10^{-8} mol L^{-1} for R6G, which is attributed to the high content of 1T-phase for the charge transfer and abundant edges to interact with the molecule. Likewise, Majee *et al.*[59] synthesized an interconnected network of vertically oriented multilayer MoS_2 nanosheets on SiO_2 by CVD and the MoS_2 nanosheets showed sensitive detection of 10^{-10} mol L^{-1} concentration of R6G and methyl orange (MO). The plenty of exposed edges enhanced light absorption and dye adsorption, thus further facilitating the interaction between MoS_2 and dyes and leading to a charge transfer resonance, resulting in the EF of 8.6×10^4 for R6G at the peak of 1 362 cm^{-1} and 5.8×10^4 for MO at 1 180 cm^{-1}. Moreover, Li *et al.*[60] compared different MoS_2 nanosheets with different interlayer distances, which were obtained by using the intercalated molecules with different sizes (L-cysteine, thiourea and glucose) *via* hydrothermal method. The MoS_2 nanosheets with 0.62 nm (termed as MoS_2−0.62), 0.87 nm (termed as MoS_2−0.87) and 1.12 nm (termed as MoS_2−1.12) interlayer distances could be synthesized by intercalating L-cysteine, thiourea and glucose, respectively. It can be found that the EF could be up to 5.31×10^5 for MoS_2−0.62, 1.44×10^5 for MoS_2−0.87 and 7.75×10^4 for MoS_2−1.12 on 4-mercaptobenzoic acid (4-MBA) probe molecule. And the SERS results of other two molecules, i.e. 4-aminothiophenol (4-ATP) and 4-mercaptopyridine (4-MPy) also exhibited that the MoS_2 with smaller interlayer distances possessed better SERS performance. According to the DFT calculation, the S-Mo bonds could serve as electron transfer paths between MoS_2 and the probe mo-

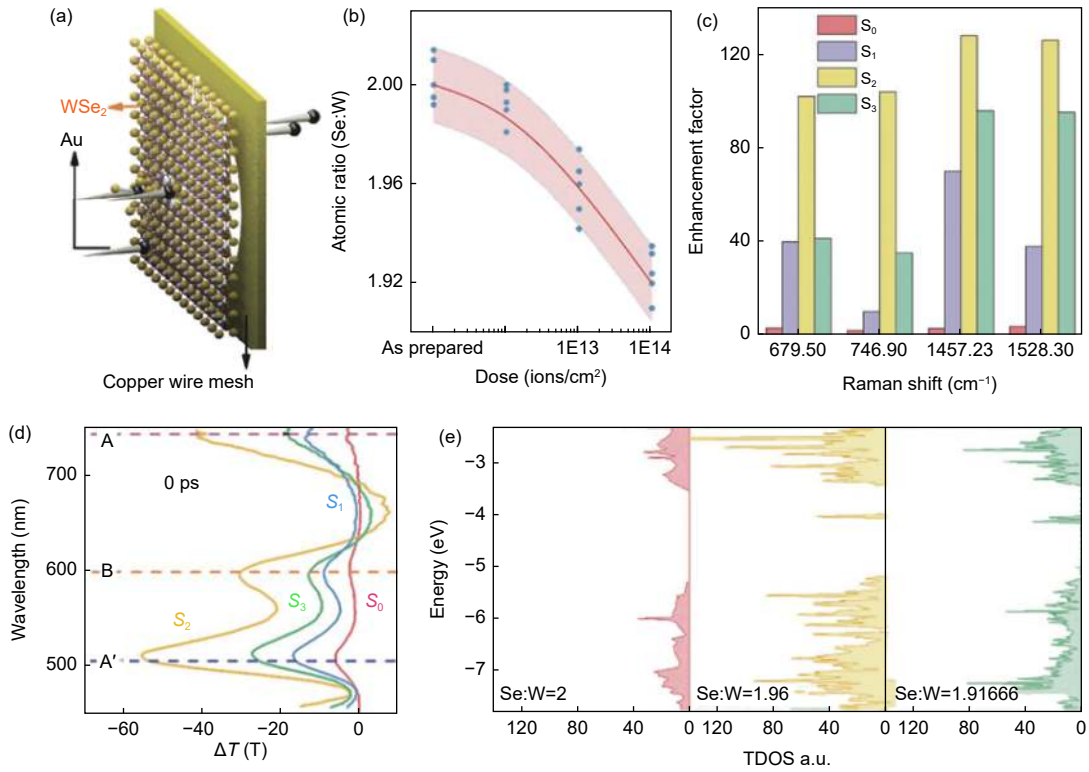

Fig. 7　(a) Schematic diagram of Au ion irradiation. (b) Evolution of atomic ratio of WSe_2 with the influence of incident ions. (c) The enhancement factor (EF) of SERS for CuPc on pristine (S_0) and irradiated WSe_2 monolayers by different controlled dose/fluence (S_1=10^{12} ions cm^{-2}, S_2=10^{13} ions cm^{-2}, S_3=10^{14} ions cm^{-2}) of ion beam. (d) The intensity of fs optical pump-probe spectroscopy at the wavelengths of 510 nm (A'), 596 nm (B) and 744 nm (A) at a time of 0 ps. (e) The total density of states (TDOS) of WSe_2 with various atomic ratios[44] (reprinted with permission from John Wiley and Sons).

lecules and more efficient interfacial charge transfer process occurred from MoS_2 nanosheets with smaller interlayer distance, which accelerated more d_{z2} orbitals of Mo elements to transform into the valence band maximum of the MoS_2/probe molecule composite, thus enhancing the Raman signal remarkably.

3.3 Other 2D layered materials

Besides graphene and TMDCs, some other 2D layered materials have also been demonstrated to be efficient SERS substrates with unique electron structures, such as BN, BP, MXenes.

h-BN is similar to graphene for the hexagonal structure and the bond length (0.144 nm of B—N and 0.142 nm of C—C) with white color so that they are called as "white graphene" sometimes. Meanwhile, it has many distinctive properties from graphene by replacing the carbon atoms in graphene with boron and nitrogen atoms[61]. The large difference in electronegativity between boron and nitrogen atoms can induce strong interfacial dipole-dipole interaction between the probe molecules and h-BN substrate, which is beneficial for SERS effect. Ling *et al.*[22] studied Raman enhancement effect on graphene, h-BN and MoS_2 for CuPc detection (Fig. 8a), they pointed out that the enhancement mechanism on h-BN was strong dipole-dipole interaction to increase matrix element *via* local symmetry-related perturbation but the charge transfer, which is different from graphene mainly by charge transfer and TMDCs by both charge transfer and weak interfacial dipole-dipole interaction. It can be explained that h-BN possesses insulating performance with a large band gap of about 5.97 eV[62], thus the electron DOS has less influence on electron transition probability for charge transfer mechanism. Therefore,

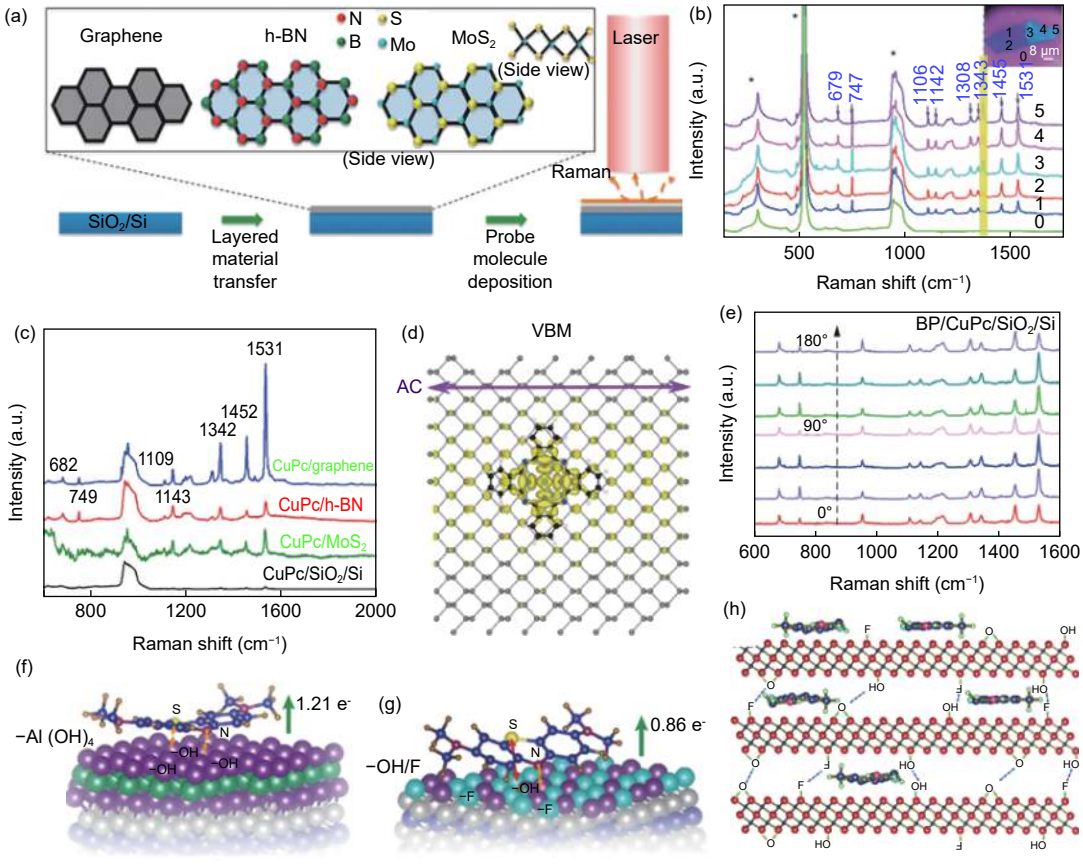

Fig. 8 (a) Schematic illustration of graphene, h-BN and MoS_2 served as SERS substrates. SERS spectra of CuPc on (b) different substrates and (c) h-BN flakes with various thicknesses[22] (reprinted with permission from American Chemical Society). (d) Charge distribution of valence band for CuPc/black phosphorus (BP) (here AC denotes armchair direction). (e) SERS spectra of CuPc on SiO_2/Si with BP[65] (reprinted with permission from American Chemical Society). Schematic illustration of charge transfer on (f) methylene blue (MB)/Ti_3C_2-$Al(OH)_4$ and (g) MB/Ti_3C_2-OH/F[70] (reprinted with permission from American Chemical Society). (h) Schematic of the adsorption and intercalation of MB in the MXene nanosheets[71] (reprinted with permission from AIP).

h-BN is a thickness independent SERS substrate because of the similar dipole interaction for various layer numbers (Fig. 8b). Ling *et al.* also found that h-BN tended to enhance lower frequency phonon modes of CuPc (like 682, 749, 1 142 and 1 185 cm^{-1}) while higher frequency phonon modes (such as 1 342, 1 452, 1 531 cm^{-1}) were increased more on graphene than on h-BN (Fig. 8c)[22]. The most attractive property of h-BN is the high thermal stability, the single layer h-BN can stabilize at more than 800 ℃ in air, which definitely shows potential to be served as reusable substrates for SERS.

Layered black phosphorus has aroused increasing interests in virtue of its high electron mobility, high biocompatibility and outstanding electronic properties[63]. It exhibits tunable bandgap dominated by thickness like graphene[64]. The most intriguing performance of BP is angle-dependent properties, the electron mobility is much higher along armchair direction than the zigzag direction owing to lower effective mass of electrons for faster charge carriers, leading to different Raman enhancement results with different orientation, as shown in Fig. 8e. When contacted with CuPc molecule, the charge near the Fermi level of BP redistributed to 1D chains along armchair direction (Fig. 8d). Besides, the photo-excited excitons in BP also tend to follow armchair direction. So that the strongest charge interaction appears only when the primary axis of the probe molecule follows armchair direction, thus leading to the largest matrix element of electron transition for the strongest Raman signal[65]. It was reported that inducing nano-void array on layered BP flake by low power focused laser irradiation could further improve the Raman enhancement (about 30%) to achieve a LOD of about 10 nmol L^{-1}[66]. The in-plane ferroelectric properties of BP favor the enhanced local electric field near the nano-voids.

At present, MXenes, a new family member of 2D materials consisting of transition metal carbides, nitrides and carbonitrides with large specific surface area and excellent electrical conductivity, have been also declared to have chemical SERS effect. MXenes are always expressed as $M_{n+1}X_nT_x$ (n=1, 2, 3), where M is transition metal, X denotes carbon or nitrogen and T_x refers to surface terminated functional group like —F, —OH and so on[67]. A simple paper supporting Ti_2N MXene SERS substrate was reported a Raman enhancement factor of 10^{12} for R6G detection, and the high enhancement of Raman signal may be attributed to the high electron density on the N atoms transferred from the Ti atoms[68]. Elumalai *et al.*[69] discovered a MXenes-enhanced resonance Raman scattering on titanium carbide film for CV molecule detection. Because of the fitted energy levels of the sensing system, the laser energy is close to the energy gap between the HOMO level of CV and the Fermi level of the MXene for electron transition (~ 1.9 eV), and the charge transfer resonance resulted in a large EF of 3.42×10^9. Furthermore, the surface metal atoms on the MXenes often show high chemical reactivities to modify with various surface functionalities on surface during the preparation, which can be applied as a convenient way to tailor the surface structure of MXenes. Ti_3C_2 sheets with $Al(OH)_4$ ligands (Ti_3C_2-$Al(OH)_4$) and OH/F ligands (Ti_3C_2-OH/F) can be obtained by the Al-extraction reaction in acid and base medium, respectively[70]. It was characterized by scanning Kelvin probe microscopy that the charge distribution on the Ti_3C_2-$Al(OH)_4$ sheets was more uniform than that on Ti_3C_2-OH/F. In general, the OH ligands would take tight interaction with N atoms on the probe molecule for hydrogen bonding, whereas the F ligands tend to show large repelling force against the atoms with high electronegativities like N and S, which locate in most dye molecules (Fig. 8f and g). Therefore, dye molecules like MB could lie flat on the Ti_3C_2-$Al(OH)_4$ sheets with strong interaction, conducive to the subsequent charge transfer. Meanwhile, the oxygen species on the surface of Ti_3C_2-$Al(OH)_4$ can protect the samples from further oxidation. Integrating the above advantages, the Ti_3C_2-$Al(OH)_4$ sheets exhibit excellent SERS effect with the LOD of pmol L^{-1} level and high stability in air. Importantly, same as graphene, MXenes were also demonstrated as thickness-dependent SERS substrates[71]. The higher posi-

tion of Fermi level of $Ti_3C_2T_x$ MXene than that of LUMO level of MB molecule benefits for charge transfer and the relatively large interlayer space of $Ti_3C_2T_x$ MXene nanosheets caused by coproducts from etching process enables the intercalation of MB to interact with all individual MXene layers (Fig. 8h), manifesting the increase of Raman enhancement with the thickness ranging from 5 to 120 nm.

3.4 Heterostructure and hybrid structure

Each material has its unique advantages, on the contrary also has its own disadvantages, designing heterostructure or hybrid structure has thus been regarded as a feasible strategy to make up the weaknesses of the individual component due to the synergistic effect. Tan *et al.*[72] stacked monolayer WSe_2 and graphene to form different heterostructure with different stacking sequence as SERS substrates, including G/W, W/G, G/W/G/W and W/G/G/W(the material in the left is close to the probe molecules). The heterostructure G/W exhibited a higher Raman intensity than pristine graphene and WSe_2 for detecting CuPc. According to the density function theory (DFT) calculation, wave functions lied in both graphene and WSe_2 for the electronic tunneling, thus increasing the DOS of the graphene for SERS. Besides, the W/G heterostructure possessed a weaker SERS than that of G/W because the WSe_2 on the top led to lower electronic transition and weaker interfacial interaction. Critically, the first layer effect for CM on 2D materials relatively limits the further improvement of SERS performance, we can find in Fig. 9a-c that the G/W/G/W and W/G/G/W showed similar SERS effect to G/W and W/G, respectively. So, it is confined to tailor the electronic properties further by stacking types. Importantly, defect engineering is also a potential strategy to tune the properties of heterostructures. Seo *et al.*[73] synthesized a graphene/ReO_xS_y vertical heterostructure as ultrasensitive substrate. The oxygen, located in the lattice structure, could induce dipole moment on the surface for complementary resonances and dipole-dipole interactions with the probe molecules (Fig. 9d). The degree of defect could be adjusted by the temperature of sulfurization for ReO_2 during the process. Together with high DOS, elaborate gap between energy levels and the interlayer coupling effect between ReO_xS_y and graphene, the vertical ReO_xS_y/graphene heterostructure demonstrated a femtomolar level Raman enhancement effect as shown in Fig. 9e. Moreover, in virtue of the excellent mechanical flexibility of the vertical heterostructure,

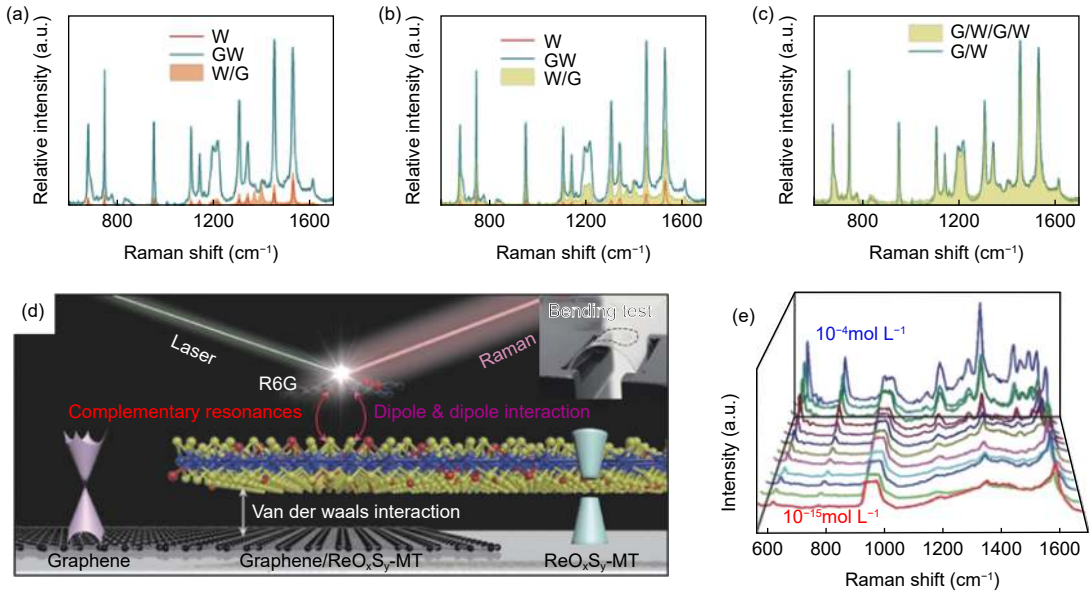

Fig. 9 (a-c) SERS spectra of CuPc on different heterostucture substrates[72] (reprinted with permission from American Chemical Society). (d) Schematic of SERS effect on graphene/ReO_xS_y heterostructure and bending test. (e) SERS spectra of R6G on graphene/ReO_xS_y vertical heterostructure[73] (reprinted with permission from American Chemical Society).

the SERS substrate can keep high sensitivity after 1 000 cycles of bending test.

More lately, 2D material coupled with noble metal nanoparticles (NPs) has been constructed as an optimized strategy for SERS, such as AuNPs/WS_2/graphene[74], AuNPs/MoS_2/graphene[75], AuNPs/GaTe[76] and so on. It was demonstrated that metal NPs decorated graphene-family nanomaterial would show pM level LOD by both CM from strong interfacial polarization and effective charge transfer and EM from metallic LSPR[77]. Besides, thanks to the negatively charged surface groups on MXenes, it is easy to absorb Au nanorods with positive charge uniformly by electrostatic self-assembly (Fig. 10a) and the SERS substrate could lead to a low LOD of 10^{-10} mol L^{-1} thiram and 10^{-8} mol L^{-1} diquat, both meet requirements of the U.S. Environmental Protection Agency, expanding the application in food safety monitoring[4]. Moreover, as shown in Fig. 10b, metal nanoparticles covered by h-BN layers could obtain a high stability in air with ultra-sensitive SERS detection[78, 79], which can still work on 2D material layers[80]. Rani *et al.*[81] induced artificial edges in monolayer MoS_2 by low-power focused laser-cutting for following deposition of AuNPs to obtain AuNPs/MoS_2 hybrid structure (Fig. 10c). The AuNPs tended to accumulate along with the edges and induced intensified plasmonic effects as hot spots, where a LOD of about 10^{-10} mol L^{-1}

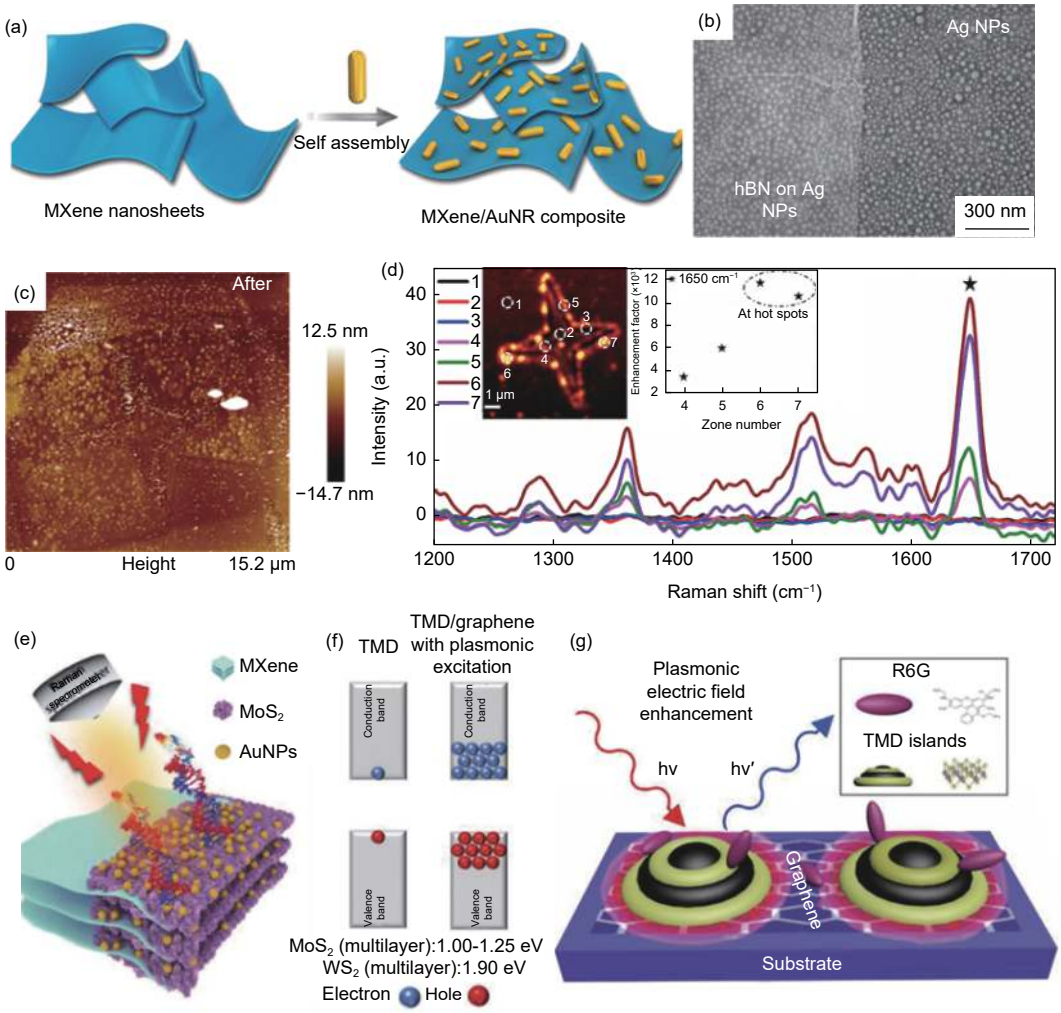

Fig. 10　(a) Schematic diagram of the fabrication of the MXene/Au nanorods (AuNRs)[4] (reprinted with permission from American Chemical Society). (b) SEM image of Ag nanoparticles (AgNPs) covered by h-BN sample[78] (reprinted with permission from John Wiley and Sons). (c) AFM topography image of laser-etched MoS_2 after decorated with AuNPs. (d) SERS spectra of RhB on various positions of AuNPs/MoS_2[81] (reprinted with permission from American Chemical Society). (e) Schematic of MXene/MoS_2@AuNPs for miRNA detection[82]. Schematic of (f) electron–hole pairs and (g) SERS mechanism of few-layer TMDs/graphene heterostructure[83] (reprinted with permission from John Wiley and Sons).

for RhB could be detected, better than that of each single material, which can be seen in Fig. 10d. In addition, miRNA, a kind of typical cancer biomarkers, may often be detected by probing DNA with generated Cyanine 5 (Cy5). Therefore, it is important to support enough DNA with high sensitivity of Cy5 for miRNA detection. Through synthesizing MXene/MoS_2@AuNPs hybrid structure, a high SERS effect for miRNA detection was achieved by Liu *et al.*[82]. As shown in Fig. 10e, the flower-like MoS_2 vertically adhering on the MXene layers provided large area to support Au nanoparticles, of which plenty of probe DNA could be adsorbed by Au–S bonds. The substrate exhibited a LOD of 10^{-9} mol L^{-1} of Cy5 with a EF of 4.8×10^8 as benchmark of substrate characteristic Raman peaks (382 cm^{-1} and 402 cm^{-1} of MoS_2 and 611 cm^{-1} of MXene). According to the DFT calculation, the gap could be a container for holes to sustain charge transfer between MXene and MoS_2 and the Fermi level of MoS_2 increased by MXene layers. Thus, both the redistributed Fermi level of the composite, which increased the electron transition probabilities due to the enlarged DOS, and the uniform distributed AuNPs "hot spots" contributed to Raman enhancement effect by both CM and EM. Especially, for some specific morphologies, TMDCs can also induce LSPR *via* photodoping, the nanostructured TMDCs may undergo photoinduced carrier doping to enhance the Raman signal *via* EM as the free carriers (both electrons and holes as shown in Fig. 10f) are excited to the CB by laser, which may also be facilitated by the dipole-dipole interaction and charge transfer in the TMDC nanodomes/graphene vdW heterostructure (Fig. 10g). Since both CM (*via* dipole-dipole interaction and charge transfer) and EM (*via* photoexcited LSPR) contributed to SERS effect, the SERS effect of R6G on TMDC nanodomes/graphene vdW heterostructure could be down to 5×10^{-12} mol L^{-1} at the peak of 613 cm^{-1}, which is 4-5 orders of magnitude higher than that of single Mo(W)S_2 (5×10^{-6} mol L^{-1}) and graphene substrate (5×10^{-7} mol L^{-1})[83]. Furthermore, the intermixed WS_2+MoS_2 nanodisks/graphene vdW heterostructure even exhibited a lower LOD of 5×10^{-13} mol L^{-1} at 613 cm^{-1} peak of R6G by the superposition of two types of LSPR effect from different plasmonic nanodisks[84]. Additionally, strain engineering is also a feasible method for 2D materials to further improve the SERS performance and the outstanding mechanical properties of 2D materials are beneficial to induce high strains. For example, Chen *et al.*[85] synthesized a wrinkled graphene/Au nanoparticles hybrid platform with a low detection level of 10^{-9} mol L^{-1} for R6G. They found that the morphology of the wrinkled graphene and the gap distance of the Au nanoparticles could be well tuned by different strains. The highest Raman intensity of 612 cm^{-1} could be obtained when the substrate was stretched by 10% tensile train. Moreover, the properties of 2D TMDCs can also be tailored by inducing strain[86, 87]. Hwang *et al.*[88] obtained multilayer MoS_2 nanoscrolls decorated with noble metal nanoparticles (Ag and Au NPs) with a high local strain, which demonstrated a high SERS enhancement factor of ~10^7. The local bending strain can not only facilitate the plasma resonance of noble metal nanoparticles but also promote the 2H to 1T phase transition of MoS_2, indicating a powerful potential of strain engineering on SERS effect.

4 Summary and perspectives

In this article, we reviewed a series of 2D inorganic layered material for SERS effect, including graphene and TMDCs, h-BN, BP and MXenes, etc (Table 1). The main SERS enhancement mechanisms consist of electromagnetic mechanism and chemical mechanism, of which the former is usually for rough metal surface with LSPR and the latter is mainly for 2D material-based substrates with charge transfer and dipole interaction. Besides, some key factors impacting the SERS effect for 2D materials are summarized, including the Fermi level, thickness, size, defect, stacking mode, orientation and so on. Based on the enhancement mechanisms, the factors can be sum up in three aspects: Fermi level, density of states and polarized interaction. Therefore, the modulation of

SERS performance can be considered based on the following aspects: (1) tune the Fermi level to match with the HOMO or LUMO energy levels of the probe molecules as fixed laser energy. (2) increase the DOS of the substrates to gain large electron transition probability. (3) facilitate strong dipole-dipole interfacial interaction for large polarization of the probe molecules. Moreover, constructing heterostructure or hybrid structure has been reported to exhibit superior SERS effect due to the efficient charge transfer between interlayers and synergistic effect with different materials. Especially when coupled with noble metal, the SERS substrates can enhance Raman signal by coupling both EM and CM. As mentioned above, 2D materials have been revealed as promising SERS substrates due to their unique electrical and optical properties with various captivating advantages and achieved ultra-high sensitivity with femtomolar level detection or even lower. However, 2D materials served as SERS platforms still face some challenges due to the relatively few researches. There is a long way to go for their practical applications and some aspects need to be well addressed in the future as below:

(1) Deep understanding of CM. 2D inorganic materials as novel SERS substrates mainly by chemical mechanisms are less studied compared to the abundant studies on noble metal rough surface as SERS substrates since its discovery in 1974, which leads to less theoretical researches on chemical mechanism for SERS. So far, there are two main models for CM, i.e. charge transfer and dipole interaction, generally supported by DFT calculation with some parameters like bandgap and DOS, which however still stays in the ambiguously qualitative interpretation and has no specific sequence of factors and concrete expression like EM. The intricate interaction among platform, probe molecule and laser energy retards to clarify inherent principles of CM-based SERS effect. Last but not the least, the variety of 2D materials with various electron structures may increase the difficulty on mechanism study, but it can also create more new opportunities to make in-depth exploration in the future.

Table 1　SERS performances and related mechanisms of various 2D materials.

Substrate	Probe molecule	Laser wavelength (nm)	Limit of detection (mol L^{-1})	Mechanism	Refs.
Graphene	CuPc	633	4×10^{-6}	Charge transfer (thickness-dependence)	[36]
Electrical field modulated graphene	CoPc	633	$<10^{-6}$		[23]
Graphene quantum dots	R6G	532	1×10^{-9}		[39]
O_2 plasma treated graphene	RhB	514	1×10^{-7}	Local dipole and charge transfer (thickness-dependence)	[33]
N-doped graphene	RhB	514	5×10^{-11}		[14]
WS_2	R6G	532	1×10^{-7}	Charge transfer and dipole-dipole interaction (thickness-dependence)	[53]
ReS_2	R6G	532	1×10^{-9}		[55]
2H-$MoS(Se)_2$	R6G	532	1×10^{-5}		[21]
1T-$MoS(Se)_2$	R6G	532	1×10^{-8}		[21]
1T'-$MoTe_2$	R6G	532	4×10^{-14}		[46]
1T'-WTe_2	R6G	532	4×10^{-15}		[46]
NbS_2	MB	633	1×10^{-14}		[54]
$NbSe_2$	R6G	532	5×10^{-16}		[57]
$SnSe_2$	R6G	532	1×10^{-17}		[51]
Hexagonal boron nitride	CuPc	633	Close to graphene	Dipole-dipole interaction (thickness-independence)	[22]
$Ti_3C_2T_x$	MB	633	1×10^{-12}	Charge transfer (thickness-dependence)	[70]
Black phosphorus with nano-void array	CuPc	532	1×10^{-8}	Charge transfer (angle-dependence)	[66]
Graphene/ReO_xS_y	R6G	532	1×10^{-15}	Charge transfer and dipole-dipole interaction	[73]
Au nanoparticles/rGO	R6G	633	1×10^{-8}	Chemical mechanism and electromagnetic mechanism	[77]
Wrinkled graphene/Au nanoparticles	R6G	633	1×10^{-9}		[85]
MXene/Au nanorods	R6G	532	1×10^{-12}		[4]
Au nanoparticles/MoS_2	RhB	532	1×10^{-10}		[81]
Mo(W)S_2 nanodomes/graphene	R6G	532	5×10^{-12}		[83]
WS_2+MoS_2 nanodisks/graphene	R6G	532	5×10^{-13}		[84]

(2) Accuracy of quantitative detection. Though more and more 2D materials have demonstrated ultra-high sensitivities with pmol L^{-1} or even fmol L^{-1} level detection, only a few studies test the performance quantitatively, among which few works show superior linearity with coefficient close to 0.999 between the peak intensity and the molecule concentration logarithm. In order to overcome the bottleneck in quantitative detection, it is of great importance to develop novel methods for robust quantified analysis technology with high precision, for instance, improve the uniformity of the as-prepared SERS substrate materials, including dispersion, size, thickness, position and even structures, so as to adsorb the probe molecules more uniformly. Critically, based on the thermodynamics and kinetics, combined with experimental and theoretical calculations, it is also necessary to reveal the adsorption process of molecules on two-dimensional material surfaces, thus guiding the design of SERS substrates for accurate quantitative detection.

(3) Exploring more probe molecule varieties. At present, the probe molecules in most researches always tend to be dye molecules for 2D material-based SERS detection, such as R6G, MB, CuPc, CV and so on, which obviously limits wider application works in other fields like biology and medicine. The low-cost, biocompatibility and flexibility capabilities of 2D material are beneficial for disposable applications like food safety, biosensor and medical diagnosis with fast response and real-time monitoring. Thus, more works on various practical probe molecules need to be devoted on 2D material-based SERS effect for widespread applications in the future.

We expect that this review will give insights on advanced and in-depth exploration on high-performance SERS substrates in the future.

Acknowledgements

This work was supported by the National Natural Science Foundation of China (Grant No. 51972191).

References

[1] Raman C V, Krishnan K S. A new type of secondary radiation[J]. Nature, 1928, 121: 501-502.

[2] Fleischmann M, Hendra P J, McQuillan A J. Raman spectra of pyridine adsorbed at a silver electrode[J]. Chemical Physics Letters, 1974, 26(2): 163-166.

[3] Zhu C, Zhao Q, Wang X, et al. Ag-nanocubes/graphene-oxide/Au-nanoparticles composite film with highly dense plasmonic hotspots for surface-enhanced Raman scattering detection of pesticide[J]. Microchemical Journal, 2021, 165: 106090.

[4] Xie H, Li P, Shao J, et al. Electrostatic self-assembly of $Ti_3C_2T_x$ MXene and gold nanorods as an efficient surface-enhanced Raman scattering platform for reliable and high-sensitivity determination of organic pollutants[J]. ACS Sensors, 2019, 4(9): 2303-2310.

[5] Li J, Koo K M, Wang Y, et al. Native microRNA targets trigger self-assembly of nanozyme-patterned hollowed nanocuboids with optimal interparticle gaps for plasmonic-activated cancer detection[J]. Small, 2019, 15(50): 1904689.

[6] Fraser J P, Postnikov P, Miliutina E, et al. Application of a 2D molybdenum telluride in SERS detection of biorelevant molecules[J]. ACS Applied Materials & Interfaces, 2020, 12(42): 47774-47783.

[7] Kim N, Thomas M R, Bergholt M S, et al. Surface enhanced Raman scattering artificial nose for high dimensionality fingerprinting[J]. Nature Communications, 2020, 11(1): 207.

[8] Kneipp K, Wang Y, Kneipp H, et al. Single molecule detection using surface-enhanced Raman scattering (SERS)[J]. Physical Review Letters, 1997, 78(9): 1667-1670.

[9] Zheng T, Zhou Y, Feng E, et al. Surface-enhanced Raman scattering on 2D Nanomaterials: Recent developments and applications[J]. Chinese Journal of Chemistry, 2021, 39(3): 745-756.

[10] Kannan P K, Shankar P, Blackman C, et al. Recent advances in 2D inorganic nanomaterials for SERS sensing[J]. Advanced Materials, 2019, 31(34): 1803432.

[11] Zhang N, Tong L, Zhang J. Graphene-based enhanced Raman scattering toward analytical applications[J]. Chemistry of Materials, 2016, 28(18): 6426-6435.

[12] Liebel M, Pazos-Perez N, Hulst N F, et al. Surface-enhanced Raman scattering holography[J]. Nature Nanotechnology, 2020, 15(12): 1005-1011.

[13] Qiu H, Wang M, Zhang L, et al. Wrinkled 2H-phase MoS_2 sheet decorated with graphene-microflowers for ultrasensitive molecular sensing by plasmon-free SERS enhancement[J]. Sensors and Actuators B:Chemical, 2020, 320: 128445.

[14] Feng S, Fantos M C, Carvalho B R, et al. Ultrasensitive molecular sensor using N-doped graphene through enhanced Raman scattering[J]. Science Advances, 2016, 2(7): e1600322.

[15] Smith E, Dent G. Modern Raman Spectroscopy: A Practical Approach [M]. England: Blackwell Science Publ, 2013.

[16] Sebastian S. Surface-enhanced Raman spectroscopy: concepts and chemical applications[J]. Angewandte Chemie-International

Edition, 2014, 53(19): 4756-4795.

[17] Laing S, Jamieson L E, Faulds K, et al. Surface-enhanced Raman spectroscopy for in vivo biosensing[J]. Nature Review Chemistry, 2017, 1(8): 60.

[18] Asing, Ali M E, Hamid S B A. SERS-modeling in molecular sensing[J]. Advanced Materials Research, 2015, 1109: 223-226.

[19] Judith L, Jimenez A D, Javier A, et al. Present and future of surface-enhanced Raman scattering[J]. ACS Nano, 2020, 14(1): 28-117.

[20] Fukui K, Kato H, Yonezawa T. A molecular orbital theory of reactivity in aromatic hydrocarbons[J]. Journal of Chemical Physics, 1952, 20(4): 722-725.

[21] Yin Y, Miao P, Zhang Y, et al. Significantly increased Raman enhancement on MoX_2 (X = S, Se) monolayers upon phase transition[J]. Advanced Functional Materials, 2017, 27(16): 1606694.

[22] Ling X, Fang W, Lee Y-H, et al. Raman enhancement effect on two-dimensional layered materials: graphene, h-BN and MoS_2[J]. Nano Letters, 2014, 14(6): 3033-3040.

[23] Xu H, Xie L, Zhang H, et al. Effect of graphene Fermi level on the Raman scattering intensity of molecules on graphene[J]. ACS Nano, 2011, 5(7): 5338-5344.

[24] Marini A, Silveiro I, Javier Garcia de Abajo F. Molecular sensing with tunable graphene plasmons[J]. ACS Photonics, 2015, 2(7): 876-882.

[25] Lv R, Li Q, Botello-Mendez A R, et al. Nitrogen-doped graphene: beyond single substitution and enhanced molecular sensing[J]. Scientific Reports, 2012, 2: 586.

[26] Novoselov K S, Geim A K, Morozov S V, et al. Electric field effect in atomically thin carbon films[J]. Science, 2004, 306(5696): 666-669.

[27] Castro Neto A H, Guinea F, Peres N M R. The electronic properties of graphene[J]. Review of Modern Physics, 2009, 81(1): 109-162.

[28] Chung C, Kim Y-K, Shin D, et al. Biomedical applications of graphene and graphene oxide[J]. Accounts of Chemical Research, 2013, 46(10): 2211-2224.

[29] Paillet M, Parret R, Sauvajol J-L, et al. Graphene and related 2D materials: An overview of the Raman studies[J]. Journal of Raman Spectroscopy, 2018, 49(1): 8-12.

[30] Ling X, Xie L, Fang, Y, et al. Can graphene be used as a substrate for Raman enhancement[J]. Nano Letters, 2010, 10(2): 553-561.

[31] Ling X, Moura, L G, Pimenta M A, et al. Charge-transfer mechanism in graphene-enhanced Raman scattering[J]. Journal of Physical Chemistry, 2012, 116(47): 25112-25118.

[32] Lv R, dos Santos M C, Antonelli C, et al. Large-area Si-doped graphene: controllable synthesis and enhanced molecular sensing[J]. Advanced Materials, 2014, 26(45): 7593-7599.

[33] Mao H, Wang R, Zhong J, et al. Mildly O_2 plasma treated CVD graphene as a promising platform for molecular sensing[J]. Carbon, 2014, 76: 212-219.

[34] Lv R, Terrones M. Towards new graphene materials: Doped graphene sheets and nanoribbons[J]. Materials Letters, 2012, 78: 209-218.

[35] Feng S, Lin, Z, Gan X, et al. Doping two-dimensional materials: ultra-sensitive sensors, band gap tuning and ferromagnetic monolayers[J]. Nanoscale Horizons, 2017, 2(2): 72-80.

[36] Ling X, Wu J, Xie L, et al. Graphene-thickness-dependent graphene-enhanced Raman scattering[J]. Journal of Physical Chemistry, 2013, 117(5): 2369-2376.

[37] Mercedes Messina M, Lorena Picone A, dos Santos Claro P C, et al. Graphene grown on Ni foam: molecular sensing, graphene enhanced Raman scattering, and galvanic exchange for surface enhanced Raman scattering applications[J]. Journal of Physical Chemistry, 2018, 122(16): 9152-9161.

[38] Zheng X, Peng Y, Yang, Y, et al. Hydrothermal reduction of graphene oxide; effect on surface-enhanced Raman scattering[J]. Journal of Raman Spectroscopy, 2017, 48(1): 97-103.

[39] Liu D, Chen X, Hu Y, et al. Raman enhancement on ultra-clean graphene quantum dots produced by quasi-equilibrium plasma-enhanced chemical vapor deposition[J]. Nature Communications, 2018, 9: 193.

[40] Huang S, Ling X, Liang L, et al. Molecular selectivity of graphene-enhanced Raman scattering[J]. Nano Letters, 2015, 15(5): 2892-2901.

[41] Ling X, Wu J, Xu W, et al. Probing the effect of molecular orientation on the intensity of chemical enhancement using graphene-enhanced Raman spectroscopy[J]. Small, 2012, 8(9): 1365-1372.

[42] Wang Q H, Kalantar-Zadeh K, Kis A, et al. Electronics and optoelectronics of two-dimensional transition metal dichalcogenides[J]. Nature Nanotechnology, 2012, 7(11): 699-712.

[43] Li Z, Jiang S, Xu S, et al. Facile synthesis of large-area and highly crystalline WS_2 film on dielectric surfaces for SERS[J]. Journal of Alloys and Compounds, 2016, 666: 412-418.

[44] Liu Y, Gao, Z, Chen M, et al. Enhanced Raman scattering of CuPc films on imperfect WSe_2 monolayer correlated to exciton and charge-transfer resonances[J]. Advanced Functional Materials, 2018, 28(52): 1805710.

[45] Lv Q, Qin X, Lv R. Controllable growth of few-layer niobium disulfide by atmospheric pressure chemical vapor deposition for molecular sensing[J]. Frontiers in Materials, 2019, 6: 279.

[46] Tao L, Chen K, Chen Z, et al. 1T′ transition metal telluride atomic layers for plasmon-free SERS at femtomolar levels[J]. Journal of the American Chemical Society, 2018, 140(28): 8696-8704.

[47] Du Z, Yang S, Li S, et al. Conversion of non-van der Waals solids to 2D transition-metal chalcogenides[J]. Nature, 2020, 577(7791): 492-496.

[48] Li W, Qian X, Li J. Phase transitions in 2D materials[J]. Nature Reviews Materials, 2021, 6: 4055.

[49] Wang Z, Li R, Su C, et al. Intercalated phases of transition metal dichalcogenides[J]. Smart Materials, 2020, 1(1): e1013.

[50] Adhikari B, Limbu T B, Vinodgopal K, et al. Atmospheric-pressure CVD growth of two-dimensional 2H- and 1T'- $MoTe_2$ films with

high-performance SERS activity[J]. Nanotechnology, 2021, 32(33): 335701.

[51] Liu M, Shi Y, Zhang, G, et al. Surface-enhanced Raman spectroscopy of two-dimensional tin diselenide nanoplates[J]. Applied Spectroscopy, 2018, 72(11): 1613-1620.

[52] Liu M, Shi Y, Wu M et al. UV surface-enhanced Raman scattering properties of $SnSe_2$ nanoflakes[J]. Journal of Raman Spectroscopy, 2020, 51(5): 750-755.

[53] Meng L, Hu S, Xu C, et al. Surface enhanced Raman effect on CVD growth of WS_2 film[J]. Chemical Physics Letters, 2018, 707: 71-74.

[54] Song X, Wang Y, Zhao F, et al. Plasmon-free surface-enhanced raman spectroscopy using metallic 2D materials[J]. ACS Nano, 2019, 13(7): 8312-8319.

[55] Miao P, Qin J-K, Shen Y, et al. Unraveling the Raman enhancement mechanism on 1T′-phase ReS_2 nanosheets[J]. Small, 2018, 14(14): 1704079.

[56] Wang L, Yu D, Huang B, et al. Large-area ReS_2 monolayer films on flexible substrate for SERS based molecular sensing with strong fluorescence quenching[J]. Applied Surface Science, 2021, 542: 148757.

[57] Lv Q, Wu X, Tan J, et al. Ultrasensitive molecular sensing of few-layer niobium diselenide[J]. Journal of Materials Chemistry A, 2021, 9(5): 2725-2733.

[58] Chen M, Ji B, Dai Z, et al. Vertically-aligned 1T/2H-MS_2 (M = Mo, W) nanosheets for surface enhanced Raman scattering with long-term stability and large-scale uniformity[J]. Applied Surface Science, 2020, 527: 146769.

[59] Majee B P, Srivastava V, Mishra A K. Surface-enhanced Raman scattering detection based on an interconnected network of vertically oriented semiconducting few-layer MoS_2 nanosheets[J]. ACS Applied Nano Materials, 2020, 3(5): 4851-4858.

[60] Li X, Guo S, Su J, et al. Efficient Raman enhancement in molybdenum disulfide by tuning the interlayer spacing[J]. ACS Applied Materials & Interfaces, 2020, 12(25): 28474-28483.

[61] Li L H, Chen Y. Atomically thin boron nitride: unique properties and applications[J]. Advanced Functional Materials, 2016, 26(16): 2594-2608.

[62] Watanabe K, Taniguchi T, Kanda H. Direct-bandgap properties and evidence for ultraviolet lasing of hexagonal boron nitride single crystal[J]. Nature Materials, 2004, 3(6): 404-409.

[63] Wang R, Yan X, Ge B, et al. Facile preparation of self-assembled black phosphorus-dye composite films for chemical gas sensors and surface-enhanced Raman scattering performances[J]. ACS Sustainable Chemistry & Engineering, 2020, 8(11): 4521-4536.

[64] Hu L, Amini M N, Wu Y, et al. Charge transfer doping modulated Raman scattering and enhanced stability of black phosphorus quantum dots on a ZnO nanorod[J]. Advanced Optical Materials, 2018, 6(15): 1800440.

[65] Lin J, Liang L, Ling X, et al. Enhanced Raman scattering on in-plane anisotropic layered materials[J]. Journal of the American Chemical Society, 2015, 137(49): 15511-15517.

[66] Kundu A, Rani R, Hazra K S. Controlled nanofabrication of metal-free SERS substrate on few layered black phosphorus by low power focused laser irradiation[J]. Nanoscale, 2019, 11(35): 16245-16252.

[67] Gu H, Xing Y, Xiong P, et al. Three-dimensional porous $Ti_3C_2T_x$ MXene-graphene hybrid films for glucose biosensing[J]. ACS Applied Nano Materials, 2019, 2(10): 6537-6545.

[68] Soundiraraju B, George B K. Two-dimensional titanium nitride (Ti_2N) MXene: synthesis, characterization, and potential application as surface-enhanced Raman scattering substrate[J]. ACS Nano, 2017, 11(9): 8892-8900.

[69] Elumalai S, Lombardi J R, Yoshimura M. The surface-enhanced resonance Raman scattering of dye molecules adsorbed on two-dimensional titanium carbide $Ti_3C_2T_x$ (MXene) film[J]. Materials Advances, 2020, 1(2): 146-152.

[70] Li G, Gong W-B, Qiu T, et al. Surface-modified two-dimensional titanium carbide sheets for intrinsic vibrational signal-retained surface-enhanced Raman scattering with ultrahigh uniformity[J]. ACS Applied Materials & Interfaces, 2020, 12(20): 23523-23531.

[71] Limbu T B, Chitara B, Cervantes M Y G, et al. Unravelling the thickness dependence and mechanism of surface enhanced Raman scattering on $Ti_3C_2T_x$ MXene Nanosheets[J]. Journal of Physical Chemistry C, 2020, 124(32): 17772-17782.

[72] Tan Y, Ma L, Gao Z, et al. Two-dimensional heterostructure as a platform for surface enhanced Raman scattering[J]. Nano Letters, 2017, 17(4): 2621-2626.

[73] Seo J, Lee J, Kim Y, et al. Ultrasensitive plasmon-free surface-enhanced Raman spectroscopy with femtomolar detection limit from 2D van der Waals heterostructure[J]. Nano Letters, 2020, 20(3): 1620-1630.

[74] Ghopry S A, Alamri M, Goul R, et al. Au nanoparticle/WS_2 nanodome/graphene van der Waals heterostructure substrates for surface-enhanced Raman spectroscopy[J]. ACS Applied Nano Materials, 2020, 3(3): 2354-2363.

[75] Alamri M, Sakidja R, Goul R, et al. Plasmonic Au nanoparticles on 2D MoS_2/graphene van der Waals heterostructures for high-sensitivity surface-enhanced Raman spectroscopy[J]. ACS Applied Nano Materials, 2019, 2(3): 1412-1420.

[76] Lu P, Lang J, Weng Z, et al. Hybrid structure of 2D layered GaTe with Au nanoparticles for ultrasensitive detection of aromatic molecules[J]. ACS Applied Materials & Interfaces, 2018, 10(1): 1356-1362.

[77] Gupta S, Banaszak A, Smith T, et al. Molecular sensitivity of metal nanoparticles decorated graphene - family nanomaterials as surface - enhanced Raman scattering (SERS) platforms[J]. Journal of Raman Spectroscopy, 2018, 49(3): 438-451.

[78] Chugh D, Jagadish C, Tan H. Large-area hexagonal boron nitride for surface enhanced raman spectroscopy[J]. Advanced Materials Technologies, 2019, 4(8): 1900220.

[79] Kim N-Y, Leem Y-C, Hong S-H, et al. Ultrasensitive and stable plasmonic surface-enhanced Raman scattering substrates covered

with atomically thin monolayers: effect of the insulating property[J]. ACS Applied Materials & Interfaces, 2019, 11(6): 6363-6373.

[80] Cai Q, Gan W, Falin A, et al. Two-dimensional Van der Waals heterostructures for synergistically improved surface-enhanced Raman spectroscopy[J]. ACS Applied Materials & Interfaces, 2020, 12(19): 21985-21991.

[81] Rani R, Yoshimura A, Das S, et al. Sculpting artificial edges in monolayer MoS_2 for controlled formation of surface-enhanced Raman hotspots[J]. ACS Nano, 2020, 14(5): 6258-6268.

[82] Liu L, Shangguan C, Guo J, et al. Ultrasensitive SERS detection of cancer-related miRNA-182 by MXene/MoS_2@AuNPs with controllable morphology and optimized self-internal standards[J]. Advanced Optical Materials, 2020, 8(23): 2001214.

[83] Ghopry S A, Alamri M A, Goul R, et al. Extraordinary sensitivity of surface-enhanced Raman spectroscopy of molecules on MoS_2 (WS_2) nanodomes/graphene van der Waals heterostructure substrates[J]. Advanced Optical Materials, 2019, 7(8): 1801249.

[84] Ghopry S A, Sadeghi S M, Farhat Y, et al. Intermixed WS_2+MoS_2 nanodisks/graphene van der Waals heterostructures for surface-enhanced Raman spectroscopy sensing[J]. ACS Applied Nano Materials, 2021, 4(3): 2941-2951.

[85] Chen W, Gui X, Zheng, Y, et al. Synergistic effects of wrinkled graphene and plasmonics in stretchable hybrid platform for surface-enhanced Raman spectroscopy[J]. Advanced Optical Materials, 2017, 5(6): 1600715.

[86] Desai S B, Seol G, Kang J S, et al. Strain-induced indirect to direct bandgap transition in multilayer WSe_2[J]. Nano Letters, 2014, 14(8): 4592-4597.

[87] Li Z, Lv Y, Ren L, et al. Efficient strain modulation of 2D materials via polymer encapsulation[J]. Nature Communications, 2020, 11(1): 1151.

[88] Hwang D Y and Suh D H. Evolution of a high local strain in rolling up MoS_2 sheets decorated with Ag and Au nanoparticles for surface-enhanced Raman scattering[J]. Nanotechnology, 2017, 28(2): 025603.

二维层状材料的表面增强拉曼散射效应及高效分子探测性能

俞凌枭[1]，　吕瑞涛[1,2,*]

（1. 清华大学 材料学院，新型陶瓷与精细工艺国家重点实验室，北京 100084；
2. 清华大学 材料学院，先进材料教育部重点实验室，北京 100084）

摘　要： 表面增强拉曼散射（SERS）因其无损检测、快速响应和高灵敏度等优点，已经发展成为一种高效的分子探测技术。但目前大多数关于 SERS 的研究仍然基于贵金属材料（如 Au、Ag 等），成本高、表面均匀性较低、生物相容性差等不足限制了其广泛应用。石墨烯具有原料来源丰富、二维原子级平面、大比表面积、高稳定性和独特的电学和光学性能等优势，研究表明其可作为一种有效的 SERS 基底材料，为相关研究开拓了新思路。近年来，过渡金属硫族化合物（TMDCs）、六方氮化硼、黑磷、二维碳氮化物等二维无机层状材料也开始受到研究者关注。本文综述了石墨烯、TMDCs 等二维层状材料作为 SERS 基底的最新研究进展并阐述了 SERS 增强机理。在此基础上，提出了二维层状材料用于高性能 SERS 基底材料研究面临的一些挑战，并对该领域发展前景进行了展望。

关键词： 石墨烯；表面增强拉曼散射；增强机理；分子探测

文章编号： 1007-8827(2021)06-0995-21　　**中图分类号：** TQ127.1$^+$1　　**文献标识码：** A

基金项目：国家自然科学基金项目（51972191）.

通讯作者：吕瑞涛，副教授. E-mail: lvruitao@tsinghua.edu.cn

作者简介：俞凌枭，博士研究生. E-mail: ylx20@mails.tsinghua.edu.cn

本文的电子版全文由 Elsevier 出版社在 ScienceDirect 上出版（https://www.sciencedirect.com/journal/new-carbon-materials/）